Available online at www.sciencedirect.com

SciVerse ScienceDirect

Journal of the Chinese Medical Association 76 (2013) 218–224

www.jcma-online.com

Original Article

Application of color-coded digital subtraction angiography in treatment of indirect carotid-cavernous fistulas: Initial experience

Chung-Jung Lin [a,b], Chao-Bao Luo [a,b], Sheng-Che Hung [a,b], Wan-Yuo Guo [a,b,*], Feng-Chi Chang [a,b], Janina Beilner [c], Markus Kowarschik [d], Wei-Fa Chu [a,b], Cheng-Yen Chang [a,b]

[a] *Department of Radiology, Taipei Veterans General Hospital, Taipei, Taiwan, ROC*
[b] *School of Medicine, National Yang-Ming University, Taipei, Taiwan, ROC*
[c] *Siemens Ltd. China, Healthcare Sector, Angiography and Interventional X-Ray Systems, Shanghai, China*
[d] *Siemens AG, Healthcare Sector, Angiography and Interventional X-Ray Systems, Forchheim, Germany*

Received June 6, 2012; accepted July 26, 2012

Abstract

Background: Parametric-colored digital subtraction angiography using Tmax is almost a routine angiographic imaging procedure, currently. The current feasibility study is aimed to using the imaging to monitor treatment effects while embolizing indirect carotid-cavernous fistulas (CCF).
Methods: Ten patients with CCFs receiving embolization and 40 patients with normal circulation time were recruited. Their color-coded DSAs were used to define the Tmax of selected intravascular ROIs. A total of 19 ROIs in the internal carotid artery (ICA) (cervical segment of ICA in AP view (I0), cavernous segment of ICA in AP view (I1), supraclinoid segment of ICA in AP view (I2) and cervical segment of ICA in lateral view (I0′), cavernous portion of ICA in lateral view (IA), supraclinoid portion of ICA in lateral view (IB)), ACA (first segment of anterior cerebral artery, second segment of anterior cerebral artery (A1, A2)), middle cerebral vein (MCA) first segment of MCA ((M1), second segment of MCA (M2)), frontal vein (FV), parietal vein (PV), superior sagittal sinus (SSS), sigmoid sinus (SS), internal jugular vein (JV), fistula, superior ophthalmic vein (SOV), inferior petrosal vein (IPS), and MCV were selected. Relative Tmax was defined as the Tmax at selected ROIs minus Tmax at I0 or I0′. An intergroup comparison between the normal and treatment groups and pre- and post-treatment comparison of the peri-therapeutic rTmax for the treatment group were performed.
Results: rTmax's for the normal group were as follows: Anterior-posterior view: I1: 0.16, I2: 0.32, A1: 0.31, M1: 0.35, SSS: 6.16, SS: 6.56, and MCV: 3.86 seconds. Lateral view: IA: 0.05, IB: 0.20, A2: 0.53, M2: 0.95, FV: 4.84, PV: 5.12, IPS: 4.62, JV: 6.81, and MCV: 3.86 seconds. Before embolization, rTmax of the IPS, SS, and JV for the treatment group were shortened ($p < 0.05$). No rTmaxs for any arterial ROIs in the fistula group were significantly different. After embolization, the rTmaxs for all venous ROIs returned to normal except for two which were partially obliterated.
Conclusion: This postprocessing method does not require extra radiation exposure and contrast media. It facilitates real-time hemodyamic monitoring and may help determining the endpoint of embolization, which increases patient safety.

Keywords: carotid-cavernous fistula; circulation time; digital subtraction angiography; embolization; hemodynamic; quantitative measurement

1. Introduction

Indirect carotid-cavernous fistulas (CCF) are abnormal connections between arteries and the cavernous sinus that lead to an altered venous drainage pathway.[1,2] Patients' symptoms are usually attributed to abnormal venous drainage.[3] The most common pathways are via the superior ophthalmic vein (SOV), inferior petrosal sinus (IPS), and infratemporal venous plexus, followed by the middle cerebral vein (MCV) and perimesencephalic veins.[4] The latter two are unusual, however, and can cause venous hypertension, subsequent venous edema, and venous infarction; they carry a higher risk of

* Corresponding author. Dr. Wan-Yuo Guo, Department of Radiology, Taipei Veterans General Hospital, 201, Section 2, Shi-Pai Road, Taipei 112, Taiwan, ROC.
E-mail address: wyguo@vghtpe.gov.tw (W.-Y. Guo).

1726-4901/$ - see front matter
http://dx.doi.org/10.1016/j.jcma.2012.12.009

ruptures with hemorrhage. Some cases involving larger shunts are more predisposed to ischemic insults because blood flow is diverted to the alternative venous channels instead of the normal distal arterial tributary.[5] One of the treatments of choice for indirect CCF is embolization, which can be performed intra-arterially, intravenously, or through direct puncture of the SOV.[6,7] Several embolizing agents are currently in use including coils, NBCA, onyx, or a combination of these.[8,9]

For pretreatment evaluation, transorbital ultrasound provides reasonable spatial and temporal resolutions of flow in the superior ophthalmic vein.[10,11] However, it cannot be used to observe the flow of the MCV, IPS, intercavernous sinus, and the venous network surrounding the brain. Phase contrast magnetic resonance angiography (MRA) can estimate blood flow but is vulnerable to sampling variation in tortuous vasculature.[12,13] It is time-consuming, and it cannot be performed within a traditional angiosuite. Modern multidetector CT angiography provides reasonable spatial resolution of vasculature, but does not provide hemodynamic information.[14–16] Although digital subtraction angiography (DSA) is invasive, it has remained the gold standard for studying complicated neurovascular disorders for the past 80 years.[17,18] In-room assessment of treatment effects within the angiosuite improves the quality of care and has become a mainstream neuro-interventional procedure.[19–21] The ideal endpoint of embolization is the complete obliteration of the shunt. In some complex CCF, complete obliteration was not feasible; however, embolized fistula showed decreased flow in the end of the secession, and developed subsequent obliteration. Recent studies have analyzed time-density curves and use time-to-maximum opacification (Tmax) to illustrate hemodynamic changes among intracranial arteriovenous malformations.[22,23] Other experimental methods utilize computerized fluid models to more accurately represent blood flows. However, these methods are computer intensive and thus not ideal for real-time monitoring.[24]

Accordingly, using parametric color-coded DSA, we hypothesized that Tmax can serve as a useful indicator to determine the endpoint of embolization for CCF patients. We conducted the current study to: (1) evaluate the diagnostic accuracy of relative Tmax (rTmax) as an indicator of intracranial circulation time with DSA; (2) compare the rTmax of patients with CCF with that of normal subjects; and (3) to monitor the effect of embolization on changes in rTmax.

2. Methods

2.1. Patient selection

From January 2011 to August 2011, patients with imaging-confirmed indirect carotid cavernous fistulas (according to the Barrow classification) referred for embolizations were retrospectively enrolled in this study. Exclusion criteria included the presence of congestive heart disease, arrhythmia, and other comorbid intracranial pathology such as carotid stenosis or intracranial aneurysms. Ten patients were available for analysis. Their clinical symptoms included red eye (70%), blurred vision (50%), diplopia (40%), and bruit (20%). No hemorrhage or other neurologic deficits were observed. There were seven males and three females; their ages ranged from 34 to 72 years old (mean = 51). All cases were treated in one session transvenously. A coil was the primary embolizing agent for all the patients; adjunctive NBCAs were used in two cases. During the same period, we enrolled another 40 patients (30 males and 10 females; mean age 54 years) with no observable intracranial circulatory disturbances as the control group. These patients were referred for DSA due to follow-up for postembolization of aneurysms, perioperative evaluation for brain tumor surgeries, and clinical suspicion of vasculitis or ischemic stroke with normal angiography findings. The institutional review board approved this study. Informed consent was obtained prior to DSA.

2.2. Imaging protocol and data analysis

A 4-French angio-catheter JB2 (Cook Inc., Bloomington, IN, USA) was placed at the level of the C4 vertebral body for common carotid angiogram both pre- and postembolization. The frame rates of anterior–posterior and lateral views were set for 6 frames/second for 12 seconds. A total volume of 12 mL bolus of a 60% diluted contrast medium (340 mg/mL) was administered for 1.67 seconds using a power injector (Liebel-Flarsheim Angiomat, Illumena, Missouri, United States). All acquisitions were acquired in the same biplane angiosuite (AXIOM-Artis, Siemens Healthcare, Forchheim, Germany). Postprocessing software (*syngo* iFlow, Siemens Healthcare, Forchheim, Germany) was used to color-code the DSA, according to the time to Tmax in seconds for each ROI. The Tmax for any selected ROI on the DSA was defined as the time point when the attenuation of the X-ray reached its maximum along the angiographic series. The diameter of a ROI was at least half of the diameter of a selected vessel. The reference time point, $t = 0$, was defined as the imaging time of the selected mask of the angiographic frames. Eight ROIs on the anterior-posterior AP view (Fig. 1A–D) and 11 ROIs on the lateral view (Fig. 2A–D) of the DSAs were defined. When an intended ROI happened to be at a vessel segment that harbored a mixture of iodinated and noniodinated blood due to confluent flows from multiple vessels or an overlapping vasculature, we repositioned the ROI to a suitable upstream or downstream location for optimal sampling. The placement of ROIs for measuring the Tmax for the 50 patients was conducted independently by two neuroradiologists. To facilitate individual comparison, we adopted the method proposed by Greitz et al and defined rTmax as Tmax at any selected ROI minus the Tmax of I0 on the AP view or the Tmax of I0′ on the lateral view of the DSA.[25]

2.3. Statistical analysis

All statistical analyses were performed using SAS 9.2 (SAS Institute Inc., Cary, NC, USA). The intraclass correlation coefficient (ICC) with a 95% confidence interval (CI) was calculated to assess the interobserver reliability of the rTmax

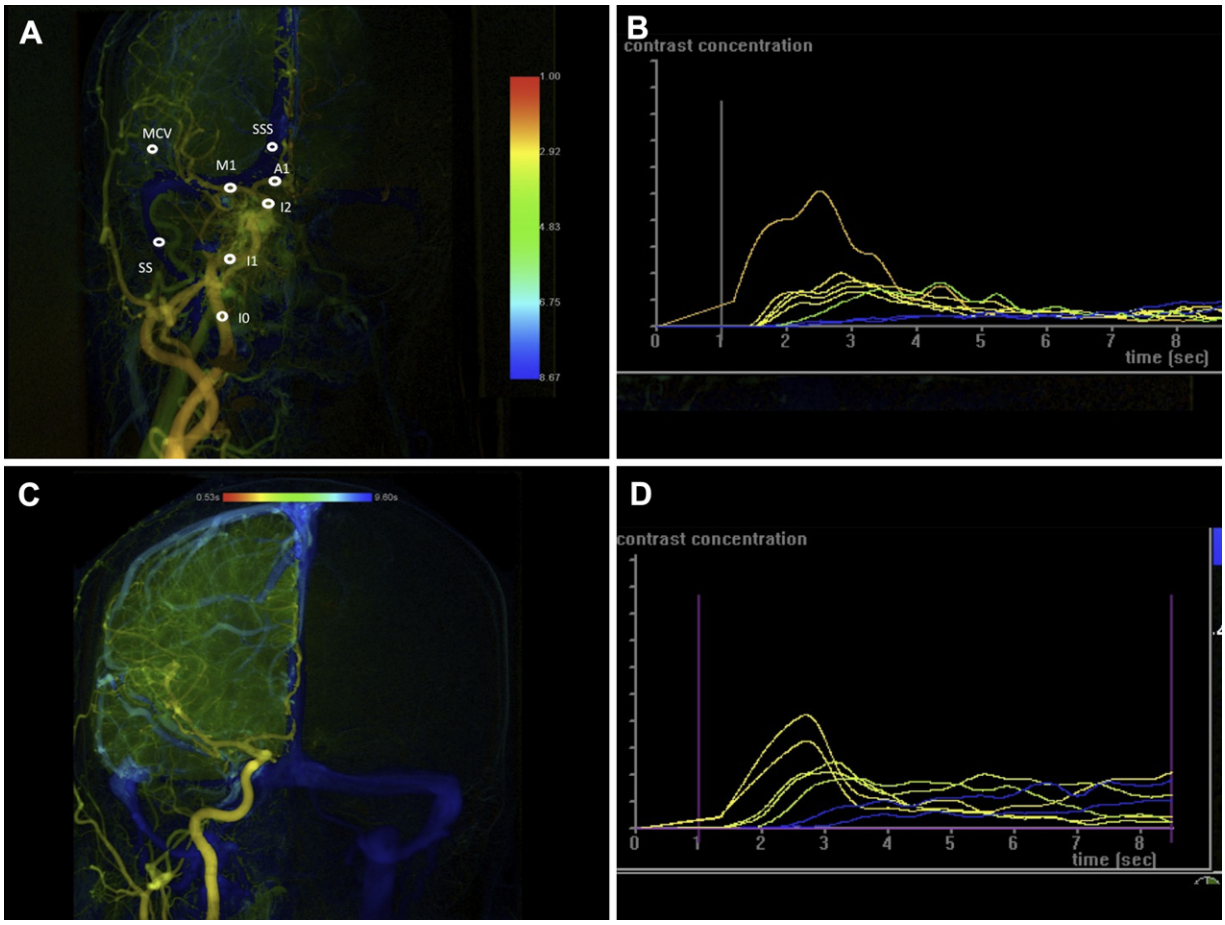

Fig. 1. (A) AP view of color-coded right carotid artery DSA of a case of carotid-cavernous fistula. (B) Time-density curves of the above-mentioned 8 ROI on AP view (horizontal axis: imaging timeline of DSA in seconds, vertical axis: contrast medium opacification). The time point of maximum contrast medium opacification of each curve is defined as the Tmax of each ROI. (C) AP view of color-coded right carotid artery DSA of a case referred for follow-up at 1 year after embolization of left posterior communicating aneurysm. The angiography showed negative findings in right CCA. (D) Time-density curve of normal AP angiogram. A1 = the midpoint of the first portion of ACA; Arterial ROI-I0 = cervical portion of ICA; I1 = cavernous portion of ICA; I2 = supraclinoid portion of ICA; M1 = the midpoint of the first segment of MCA; MCV = the midpoint of the ascending limb of MCV; SS = the midpoint of sigmoid sinus; venous ROI-SSS = a point located 2 cm above the torcular herophili.

measurements. ICC values were interpreted using the following scale: almost perfect (1.00–0.8), substantial (0.8–0.6), moderate (0.6–0.4), fair (0.4–0.2), and slight (<0.2, with no significant correlation in rTmax measurements between the two observers if the 95% CI covers zero). The rTmax difference between the fistula and control groups and longitudinal changes of rTmax during the embolization were examined using the Wilcoxon rank sum test. Significance was set at $p = 0.05$.

3. Results

There were seven cases of Barrow type C CCF, and three cases of Barrow type D CCF. The rTmax measurements at the arterial ROIs showed substantial agreement (0.61–0.76) between the two neuroradiologists except for A2 (ICC = 0.530, CI: 0.186–0.639) and M2 (ICC = 0.560, CI: 0.101, 0.713), which showed moderate agreement. Among the venous ROIs, MCV, SSS, fistula and IPS showed substantial agreement (ICCs ranged from 0.61 to 0.63); whereas SS, FV, PV, and SOV showed moderate agreement (ICC ranged from 0.45 to 0.57) (Table 1). The mean rTmax of all ROIs in the control and pre-embolization patient groups are listed in Table 2. Before embolization, all rTmax of the ROIs located in the ICA on AP and lateral views were shortened but this effect did not reach significance. Among the venous ROIs, only IPS, SS, and JV were significantly shortened, indicating increased blood flow due to shunts.

The rTmaxs of all ROIs before and after embolization are listed in Table 3. After embolization, the rTmax of the venous ROIs in IPS, SS, and JV were normalized, but this effect only achieved significance for the SS and JV ROIs. The rTmax was not available for the eight completely embolized fistulas (as the embolizing agent made imaging impossible). Disappearance of the SOV was observed in all eight cases due to closure of shunts. The rTmax of the SOV and IPS for the two partially embolized fistulas were prolonged. Both still demonstrated faint visible arterial feeders and drainage veins (Fig. 3A–D). However, the obliteration of both fistulas was confirmed during control angiography at 4 and 6 months, respectively. As a group, postembolization

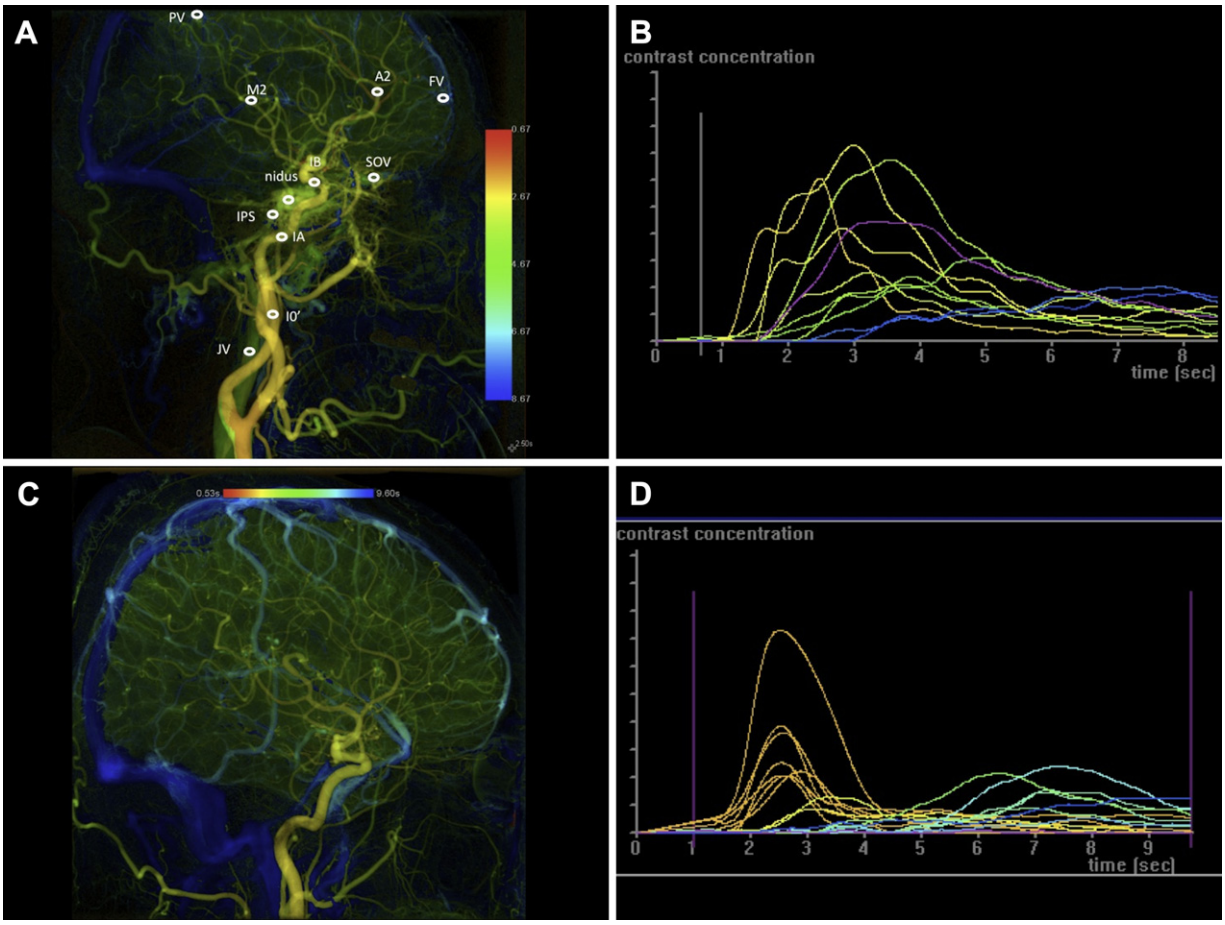

Fig. 2. (A) Lateral view of a color-coded right carotid artery DSA of a case of carotid-cavernous fistula. The venous ROI of FV, PV, SOV, and IPS are designated at the biggest diameter within the visible field; the fistula is located at the uncovered cavernous sinus, and JV is located at a point 2 cm below its junction with SS. (B) Time-density curves of the above-mentioned 11 ROI on lateral view. These arterial ROIs showed widened waves and two peaks due to turbulence and diversions of blood flow toward the shunt as compared with the control group (see Fig. 2D). (C) Lateral view of color-coded right carotid artery DSA of a case referred for follow-up at 1 year after embolization of the left posterior communicating aneurysm. The angiography showed negative findings in the right CCA. (D) Time-density curve of normal lateral angiogram. IA = cavernous portion of ICA; IB = supraclinoid portion of ICA; A2 = the midpoint of the second portion of ACA; Arterial ROI-I0′ = cervical portion of ICA; M2 = a point in the proximal temporal branch of MCA before its bifurcation.

Table 1
Interobserver reliability of rTmax measurements at different ROI.

	ROI	ICC (95% CI)
AP view		
Arterial ROI	I1	0.760 (0.508, 0.941)
	I2	0.750 (0.424,0.933)
	A1	0.610 (0.169, 0.856)
	M1	0.540 (0.232, 0.773)
Venous ROI	MCV	0.630 (0.086, 0.742)
	SSS	0.680 (0.393, 0.846)
	SS	0.545 (−0.255, 0.857)
Lateral view		
Arterial ROI	Ia	0.730 (0.488, 0.926)
	Ib	0.710 (0.395, 0.805)
	A2	0.530 (0.186, 0.639
	M2	0.560 (0.101, 0.713)
Venous ROI	FV	0.450 (−0.195, 0.566)
	PV	0.480 (−0.192, 0.846)
	SOV	0.570 (−0.068, 0.699)
	IPS	0.610 (−0.164, 0.832)
	JV	0.560 (−0.084, 0.620)
	Fistula	0.650 (−0.08, 0.868)

ICC = intraclass correlation coefficients; CI = confidence interval.

rTmax of sigmoid sinus was normalized and did not differ from the normal group. There was no correlation between the rTmaxs and the feeding artery, drainage vein, or number of coils used.

4. Discussion

The weaker correlation of rTmax in venous ROIs as compared with those in arterial ROIs between two observations was likely caused by the more heterogenous dilution of contrast in the veins than in the arteries. This phenomena will be more evident in the major sinuses. Another possible explanation is that the change of the time-density curve in the veins is less prominent compared with that in the arteries, thus making identification of Tmax more challenging. The wide variation of Tmax in the ICA in those patients with CCF may be attributed to the turbulent flow in the vicinity of the shunts. In reality, the flows within the vessels are not spatially or temporally homogenous due to their laminated nature and their turbulent properties during propagation. These flow patterns

Table 2
Comparison of the average rTmax of each ROI in indirect patients with carotid cavernous fistulas versus the control group.

	Patient group (pre-embolization, $n = 10$)	Control group ($n = 40$)	p (Wilcoxon rank sum test)
AP view			
I1	0.23 ± 0.50	0.16 ± 0.25	0.42
I2	0.32 ± 0.67	0.32 ± 0.27	0.96
A1	0.31 ± 0.53 ($n = 8$)	0.31 ± 0.28 ($n = 18$)	0.70
M1	0.30 ± 0.54	0.35 ± 0.37	0.75
SSS	5.66 ± 1.57	6.16 ± 1.14	0.37
SS	4.99 ± 2.36	6.56 ± 2.54	0.03*
MCV	3.49 ± 1.82	3.86 ± 1.70	0.23
Lateral view			
IA	0.06 ± 0.47	0.05 ± 0.23	0.87
IB	0.28 ± 0.61	0.20 ± 0.22	0.5
A2	0.44 ± 0.76 ($n = 8$)	0.53 ± 0.34 ($n = 18$)	0.10
M2	1.20 ± 0.77	0.95 ± 0.35	0.07
FV	6.16 ± 2.56	4.84 ± 1.11	0.45
PV	5.14 ± 1.68	5.12 ± 1.18	0.35
SOV	2.20 ± 0.92	N/A	N/A
IPS	2.36 ± 2.28 ($n = 9$)	4.62 ± 1.53 ($n = 31$)	0.02*
JV	5.10 ± 2.57	6.81 ± 1.25	0.048*
Fistula	0.26 ± 1.42	N/A	N/A

*Statistically significant ($p < 0.05$) by Wilcoxon rank sum test.
FV = frontal vein; I0 = cervical segment of ICA in AP view; I0′ = cervical segment of ICA in lateral view; I1 = cavernous segment of ICA in AP view; I2 = supraclinoid segment of ICA in AP view; IA = cavernous portion of ICA in lateral view; IB = supraclinoid portion of ICA in lateral view; ICA = internal carotid artery; IPS = inferior petrosal vein; JV = internal jugular vein; MCV = middle cerebral vein; PV = parietal vein; SOV = superior ophthalmic vein; SS = sigmoid sinus; SSS = superior sagittal sinus.

Table 3
Comparison of the average rTmax of each ROI in patients with indirect carotid-cavernous fistulas before and after embolization.

	Before embolization ($n = 10$)	After embolization ($n = 10$)	p (Wilcoxon rank sum test)
AP view			
I1	0.23 ± 0.50	0.23 ± 0.42	1.0
I2	0.32 ± 0.67	0.28 ± 0.58	0.92
A1	0.31 ± 0.53 ($n = 8$)	0.58 ± 0.31	0.45
M1	0.30 ± 0.54	0.63 ± 0.52	0.10
SSS	5.66 ± 1.57	6.94 ± 2.06	0.11
SS	4.99 ± 2.36	7.31 ± 1.62	0.028*
MCV	3.49 ± 1.82	3.49 ± 3.23	0.86
Lateral view			
IA	0.06 ± 0.47	0.05 ± 0.41	0.66
IB	0.28 ± 0.61	0.28 ± 0.58	0.66
A2	0.44 ± 0.76 ($n = 8$)	0.23 ± 0.86 ($n = 8$)	0.13
M2	1.20 ± 0.77	1.05 ± 0.74	0.06
FV	6.16 ± 2.56	6.43 ± 1.25	0.89
PV	5.14 ± 1.68	5.36 ± 1.50	0.62
SOV	2.20 ± 0.92	3.01 ± 0.65 ($n = 2$)	0.18
IPS	2.36 ± 2.28 ($n = 9$)	4.62 ± 2.16 ($n = 6$)	0.753
JV	5.10 ± 2.57	7.08 ± 2.00	0.02*
Fistula	0.26 ± 1.42	1.34 ± 1.48 ($n = 2$)	0.47

*Statistically significant ($p < 0.05$) by Wilcoxon rank sum test.
FV = frontal vein; I0 = cervical segment of ICA in AP view; I0′ = cervical segment of ICA in lateral view; I1 = cavernous segment of ICA in AP view; I2 = supraclinoid segment of ICA in AP view; IA = cavernous portion of ICA in lateral view; IB = supraclinoid portion of ICA in lateral view; ICA = internal carotid artery; IPS = inferior petrosal vein; JV = internal jugular vein; MCV = middle cerebral vein; PV = parietal vein; SOV = superior ophthalmic vein; SS = sigmoid sinus; SSS = superior sagittal sinus.

may explain the variances in the measurement of rTmax. To overcome this disadvantage, we used the ROIs of selected vessels to minimize the inhomogeneity.

Previous literature has proposed prolonged circulation time for the affected hemisphere due to arterial "stealing," which occurs when the larger shunt diverts inflow contrast and thus diminishes the accumulation of contrast distally.[26] We observed this phenomenon in only one case. Our explanation is that all of our cases were indirect type CCFs, which caused less prominent shunting and thus had less impact on intracranial circulation. There were two cases with residual shunt and stagnant flow immediate postembolization, but in both cases, complete obliteration of the fistula was confirmed during follow-up. Due to limited number, rTmax in fistula, SOV, and IPS were prolonged, but failed to achieve statistical significance. However, it seems that prolonged rTmax real-time can quantitatively reflect the decreased flow as we approach the endpoint of the embolization. This is extremely important during the treatment of indirect CCFs to avoid unnecessarily aggressive embolization. Most of the time, indirect CCFs receive numerous fine arterial feeders, and thus complete obliteration is not always possible in immediate control angiography.

The polymorphic waveforms of arterial ROIs was caused by the flow diversion of the fistula, which hindered the summation effect of the contrast in the arterial downstream flow and thus prolonged the transit time. This phenomenon became less evident during the embolization process.

The major advantage of using time-density curves to analyze the flow is that this method is less time consuming than computed fluid dynamic simulation. Immediate flow analysis is mandatory during peritherapeutic application in order to minimize operation time and the associated risk of thromboembolism events. A second advantage is that no extra radiation and contrast medium need be given because the data were all processed after the completion of routine DSA acquisition. However, the major drawback of this algorithm is that it provides less accurate 2D information. To minimize the effect of individual cardiac output while evaluating the time-density curve, we adopted rTmax standardized by the circulation time of the brain, as proposed by Greitz et al,[25] to eliminate the time variances that may stem from the contrast medium travelling between the heart and cervical ICA.[25,26] It is highly reproducible and contains the lowest systemic error between different observers and patient populations. The other advantage is that rTmax is correlated linearly to CBF in the corresponding area. Recent correlation of CT perfusion and DSA also confirmed

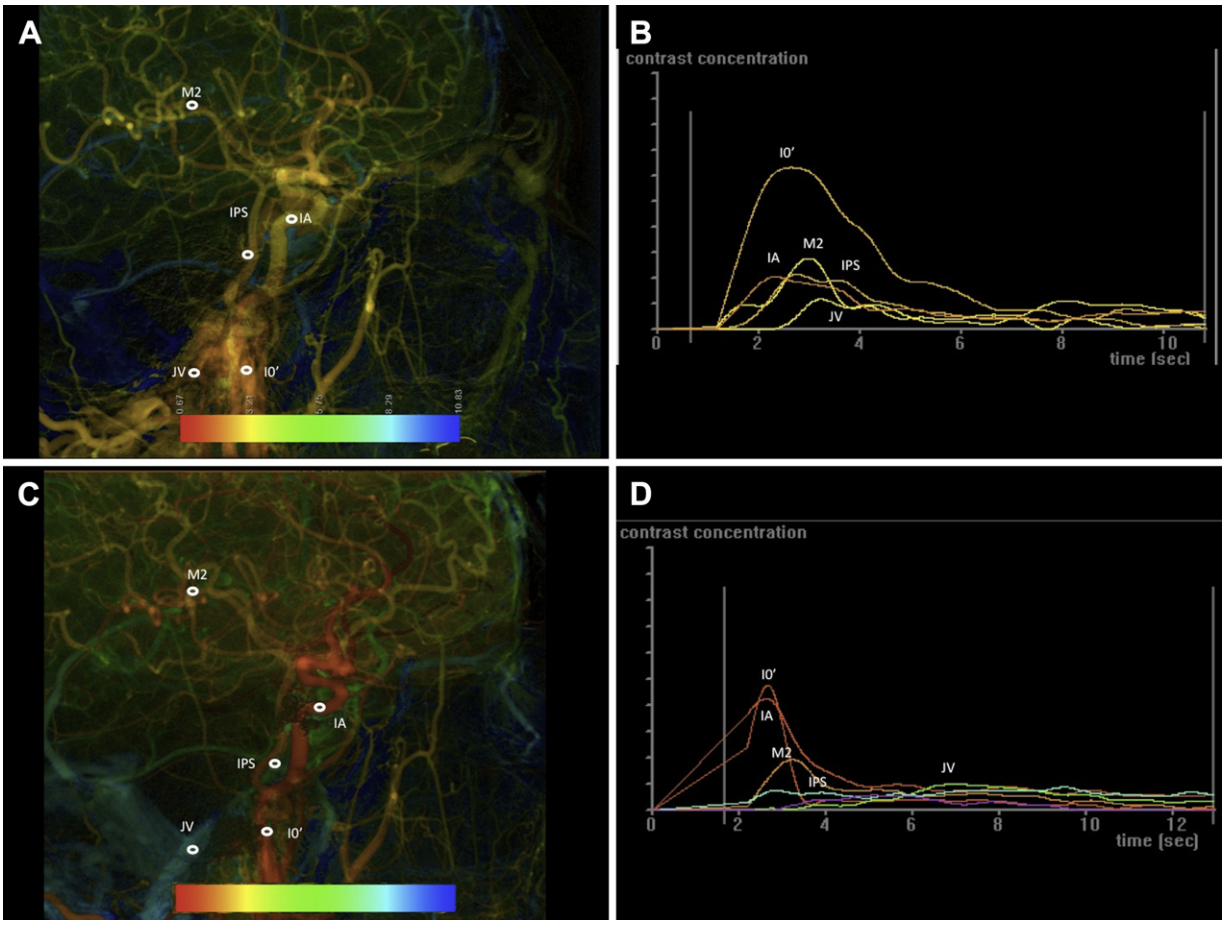

Fig. 3. (A) Lateral view of color-coded left carotid artery DSA of a 30-year-old male with indirect CCF at the left proximal ICA. Before embolization, five selected ROIs in the following order: cervical portion of ICA (I0), cavernous portion of ICA (IA), the temporal branch of MCA (M2), IPS, and JV. (B) Time-density curves of the selected ROI in (A). The waveform of IA is relatively wider and showed two peaks as compared with that of M2. (C) Lateral view of the color-coded left carotid artery DSA of the same patient after partial embolization. The same 5 selected ROI as in (A). (D) After embolization, the time–density curves of the arterial ROIs became narrower. Their Tmax of IPS and SSS were also prolonged and returned to normal.

these findings.[27] Both studies demonstrated that rTmax is a reliable hemodynamic marker of the brain.

There are some limitations to the present study. First, the size of the treatment group is small. Although elongation of the venous rTmax implies future closure of shunts, a larger number of cases is needed to validate the optimal cut-off values between shunts and normal groups. Second, the turbulence and diversions of flow caused by the fistula produce multiple fluctuating ascending and declining contrast medium peaks along the time-density curves, and complicate the Tmax determination. First arrival time of the contrast can serve as an alternative reference in this condition; unfortunately, our current version does not provide this information on the color-coding map. Third, due to the high flow nature of a CCF, intravascular flow measurement of the arterial ROI is beyond the scope of our current frame rate (6 frames/second). A higher frame rate with appropriate radiation reduction techniques are needed for further investigation. Fourth, DSA is basically two-dimensional imaging. Overlapping and collapsing all vasculatures on a two-dimensional projection, e.g., cavernous portion of the ICA on an AP view and the proximal MCA on a lateral view, can accentuate the contrast medium density and mistakenly shift the Tmax. The exact registration of flow changes of each voxel in the 3D anatomic positions would be the ultimate means of overcoming the constraints of two-dimensionality.[28–31] However, this is beyond the power of the current mechanics and would result in too much radiation exposure.[32,33]

In conclusion, this study confirmed the feasibility of using rTmax to quantify the altered venous flow in patients with indirect CCFs. It can serve as a good hemodynamic marker to monitor therapeutic effects of embolization while treating patients with indirect CCFs. Color-coded DSA provided improved visualized differences and quantitative changes in blood flow in-room and real-time, on a single image, without requiring additional contrast medium and radiation exposure. It is proposed that this may help in the management of intracranial vascular diseases.

Acknowledgments

We would like to thank Eric C.S. Lin for his assistance with the statistical analysis, and Victoria Chen for her editing in English. This research was in part cosponsored by Taipei

Veterans General Hospital and Siemens Healthcare (grant number: T1100200).

References

1. Sommer C, Müllges W, Ringelstein EB. Noninvasive assessment of intracranial fistulas and other small arteriovenous malformations. *Neurosurgery* 1992;**30**:522−8.
2. Luo CB, Teng MM, Chang FC, Chang CY, Guo WY. Traumatic indirect carotid cavernous fistulas: angioarchitectures and results of transarterial embolization by liquid adhesives in 11 patients. *Surg Neurol* 2009;**71**: 216−22.
3. Higashida RT, Halbach VV, Tsai FY, Norman D, Pribram HF, Mehringer CM, et al. Interventional neurovascular treatment of traumatic carotid and vertebral artery lesions: results in 234 cases. *Am J Roentgenol* 1989;**153**:577−82.
4. Th'eaudin M, Audin M, Chapot R, Vahedi K, Bousser MG. Dural carotid-cavernous fistula: relationship between evolution of clinical symptoms and venous drainage changes. *Cerebrovasc Dis* 2008;**25**: 382−4.
5. Murata H, Kubota T, Murai M, Kanno H, Fujii S, Yamamoto I. Brainstem congestion caused by direct carotid-cavernous fistula—case report. *Neurol Med Chir(Tokyo)* 2003;**43**:255−8.
6. Luo C, Teng M, Lin C, Chang F, Chang C. Direct puncture of a prematurely detached balloon in the supraclinoid ICA via the optic canal during embolisation of a traumatic carotid-cavernous fistula. *Acta Neurochir (Wien)* 2010;**152**:321−4.
7. Lin C, Luo C, Chang F, Teng M, Wang K, Chu S. Combined transarterial, transvenous, and direct puncture of the cavernous sinus to cure a traumatic carotid cavernous fistula. *J Clin Neurosci* 2009;**16**:1663−5.
8. Luo CB, Teng MM, Chang FC, Chang CY. Endovascular treatment of intracranial high-flow arteriovenous fistulas by Guglielmi detachable coils. *J Chine Med Assoc* 2006;**69**:80−5.
9. Elhammady MS, Wolfe SQ, Farhat H, Moftakhar R, Aziz-Sultan MA. Onyx embolization of carotid-cavernous fistulas. *J Neurosurg* 2010;**112**: 589−94.
10. Duan Y, Liu X, Zhou X, Cao T, Ruan L, Zhao Y. Diagnosis and follow-up study of carotid cavernous fistulas with color Doppler ultrasonography. *J Ultras Med* 2005;**24**:739−45.
11. Heggerick PA, Hedges TR. The role of color Doppler imaging in assessing carotid cavernous fistulas and dural arteriovenous shunts. *J Vasc Tech* 1998;**22**:157−61.
12. Brisman JL, Pile-Spellman J, Konstas AA. Clinical utility of quantitative magnetic resonance angiography in the assessment of the underlying pathophysiology in a variety of cerebrovascular disorders. *Eur J Radiol* 2012;**81**:298−302.
13. Hope TA, Hope MD, Purcell DD, von Morze C, Vigneron DB, Alley M, et al. Evaluation of intracranial stenoses and aneurysms with accelerated 4D flow. *Magn Reson Imaging* 2010;**28**:41−6.
14. Petkova M, Gauvrit JY, Trystram D, Nataf F, Godon-Hardy S, Munier T, et al. Three-dimensional dynamic time-resolved contrast-enhanced MRA using parallel imaging and a variable rate k-space sampling strategy in intracranial arteriovenous malformations. *J Magn Reson Im* 2009;**29**:7−12.
15. Siebert E, Bohner G, Dewey M, Masuhr F, Hoffmann KT, Mews J, et al. 320-slice CT neuroimaging: initial clinical experience and image quality evaluation. *Br J Radiol* 2009;**82**:561−70.
16. Roth C. Value of CT and MR angiography for diagnostics of intracranial aneurysms. *Der Radiologe* 2011;**51**:106−12.
17. Raney R, Raney AA, Sanchez-Perez JM. The role of complete cerebral angiography in neurosurgery. *J Neurosurg* 1949;**6**:222−37.
18. Curtis JB. Rapid serial angiography; preliminary report. *J Neurol Neurosur Psychiatry* 1949;**12**:167−81.
19. Hamstra DA, Chenevert TL, Moffat BA, Johnson TD, Meyer CR, Mukherji SK, et al. Evaluation of the functional diffusion map as an early biomarker of time-to-progression and overall survival in high-grade glioma. *Proc Natl Acad Sci U S A* 2005;**102**:16759−64.
20. Struffert T, Deuerling-Zheng Y, Kloska S, Engelhorn T, Strother CM, Kalender WA, et al. Flat detector CT in the evaluation of brain parenchyma, intracranial vasculature, and cerebral blood volume: a pilot study in patients with acute symptoms of cerebral ischemia. *Am J Neuroradiol* 2010;**31**:1462−9.
21. Struffert T, Ott S, Adamek E, Schwarz M, Engelhorn T, Kloska S, et al. Flat-detector computed tomography in the assessment of intracranial stents: comparison with multidetector CT and conventional angiography in a new animal model. *Eur Radiol* 2011;**21**:1779−87.
22. Strother CM, Bender F, Deuerling-Zheng Y, Royalty K, Pulfer KA, Baumgart J, et al. Parametric color coding of digital subtraction angiography. *Am J Neuroradiol* 2010;**31**:919−24.
23. Cover KS, Lagerwaard FJ, van den Berg R, Buis DR, Slotman BJ. Color intensity projection of digitally subtracted angiography for the visualization of brain arteriovenous malformations. *Neurosurgery* 2007;**60**:511−4. discussion 514−515.
24. Shpilfoygel SD, Close RA, Valentino DJ, Duckwiler GR. X-ray videodensitometric methods for blood flow and velocity measurement: a critical review of literature. *Med Phys* 2000;**27**:2008−23.
25. Greitz T. A radiologic study of the brain circulation by rapid serial angiography of the carotid artery. *Acta Radiol* 1956;(140 Suppl):1−123.
26. Fabian TS, Woody JD, Ciraulo DL, Lett ED, Phlegar RF, Barker DE, et al. Posttraumatic carotid cavernous fistula: frequency analysis of signs, symptoms, and disability outcomes after angiographic embolization. *J Trauma* 1999;**47**:275−81.
27. Aikawa H, Kazekawa K, Tsutsumi M, Onizuka M, Iko M, Kodama T, et al. Intraprocedural changes in angiographic cerebral circulation time predict cerebral blood flow after carotid artery stenting. *Neurol Med Chir(Tokyo)* 2010;**50**:269−74.
28. Söderman M, Babic D, Holmin S, Andersson T. Brain imaging with a flat detector C-arm: technique and clinical interest of XperCT. *Neuroradiology* 2008;**50**:863−8.
29. Strobel N, Meissner O, Boese J, Brunner T, Heigl B, Hoheisel M, et al. *3D imaging with flat-detector C-arm systems multislice CT*. Berlin, Germany: Springer; 2009.
30. Hawkes DJ, Seifalian AM, Colchester AC, Iqbal N, Hardingham CR, Bladin CF, et al. Validation of volume blood flow measurements using three-dimensional distance-concentration functions derived from digital x-ray angiograms. *Invest Radiol* 1994;**29**:434−42.
31. Heran NS, Song JK, Namba K, Smith W, Niimi Y, Berenstein A. The utility of DynaCT in neuroendovascular procedures. *Am J Neuroradiol* 2006;**27**:330−2.
32. Lin C-J, Blanc R, Clarencon F, Piotin M, Spelle L, Guillermic J, et al. Overlying fluoroscopy and preacquired CT angiography for road-mapping in cerebral angiography. *Am J Neuroradiol* 2010;**31**:494−5.
33. Mistretta CA. Sub-Nyquist acquisition and constrained reconstruction in time resolved angiography. *Med Phys* 2011;**38**:2975−85.